PCCP

PAPER

View Article Online
View Journal | View Issue

Cite this: *Phys. Chem. Chem. Phys.*, 2018, **20**, 26325

$C_{50}Cl_{10}$, a planar aromatic fullerene. Computational study of ^{13}C-NMR chemical shift anisotropy patterns and aromatic properties†

Alan Miralrio,[a] Luis E. Sansores,[b] Bruce King[c] and Alvaro Muñoz-Castro*[d]

Received 2nd August 2018,
Accepted 17th September 2018

DOI: 10.1039/c8cp04938f

rsc.li/pccp

The isolated-pentagon-rule (IPR) is a prime determinant of fullerene stabilization accounting for the difficult isolation of hollow C_n ($n < 60$) species. In this connection, the isolation and structural characterization of D_{5h}-$C_{50}Cl_{10}$ as an IPR-violating fullerene are of interest owing to the study of factors providing further stability. Herein, we use DFT calculations to explore its aromatic behavior. In this connection the $C_{50}Cl_{10}$ structure is considered as a fullerene displaying a planar-aromatic character provided by the face-to-face disposition of two IPR structural motifs, mediated by ten exobonded sp^3-carbons. In addition, the D_{5h}-$C_{50}Br_{10}$ counterpart appears to be another promising structure as the target for explorative synthesis. Owing to the curvature of its IPR motif, an interesting variation in the ^{13}C-NMR patterns relative to corannulene is described, where the relation between C_I and C_{II} signals is useful to evaluate the degree of the curvature of the π-surface. The charge distribution of $C_{50}Cl_{10}$ reveals a more electron-deficient IPR dome in comparison to C_{60}, envisaging an enhanced chemistry related to bare fullerenes. In addition, the –Cl and –Br exobonded atoms provide effective σ-holes, suggesting such oblate fullerenes as interesting two-dimensional five-fold symmetric synthons useful for the formation of supramolecular species. Hence, an interesting chemistry and supramolecular array derivatives are potential applications to be further explored towards the development of novel nano-devices.

Introduction

The initial observation of buckminsterfullerene, C_{60},[1–4] resulted from Kroto's research interest in microwave spectroscopy of outer-space[5] carbon structures. Subsequent research led to the development of its large scale synthesis.[6] The unusual highly symmetrical C_{60} structure has stimulated several research efforts directed towards understanding the relationship between such polyhedral structures and fullerene stability.[7–13]

The truncated icosahedral structure of C_{60} consists of 12 pentagonal rings and 20 hexagonal rings satisfying the requirements for a roughly spherical shape, resulting in a pleasant aesthetic cage obeying the isolated-pentagon rule (IPR).[14,15] Usually, the stability has been related to the IPR, where C_{60} is the smallest carbon cluster able to fulfill the IPR requirement. In this sense, hollow C_n fullerenes smaller than C_{60} including C_{20}, C_{28}, and C_{36}[16–22] are highly reactive species owing to the necessary presence of fused pentagon motifs.[23,24] Such structural features lead to higher strain thereby making fullerenes smaller than C_{60} difficult to isolate, thus preventing the exploration of their chemistry. However, some medium-sized fullerenes smaller than C_{60} necessarily violating the IPR rule can be stabilized by saturation of a few sp^2 cagecarbon atoms by bonding them to external atoms or groups.

An example of such stabilization of an IPR-violating fullerene was provided in 2004 by the discovery, isolation, and characterization of $C_{50}Cl_{10}$ by Xie and coworkers[25] as representing the stabilization of the IPR-violating D_{5h} isomer of C_{50} by introducing ten external symmetrically placed chlorine atoms, as part of a series of halogenated fullerenes detected and explored in the same decade,[26] as for example $C_{60}F_{18}$ with interesting aromatic properties.[27–30] The initial characterization of $C_{50}Cl_{10}$, provided by mass spectroscopy and ^{13}C-NMR allowing the unequivocal deduction of its molecular structure, was later confirmed by X-ray crystallography.[31] Noteworthily, the stabilized $C_{50}Cl_{10}$ cage exhibits an oblate D_{5h}-C_{50} structure in which chlorine atoms saturate the equatorial atoms, thereby

[a] *Departamento de Física y Química Teórica, DEPg. Facultad de Química, Universidad Nacional Autónoma de México, UNAM, Del. Coyoacán, Ciudad de México 04510, Mexico*
[b] *Departamento de Materiales de Baja Dimensionalidad, Instituto de Investigaciones en Materiales, UNAM, Apartado Postal 70-360, Ciudad de México 04510, Mexico*
[c] *Department of Chemistry, University of Georgia, Athens, Georgia 30602, USA*
[d] *Grupo de Química Inorgánica y Materiales Moleculares, Universidad Autonoma de Chile, El Llano Subercaseaux 2801, Santiago, Chile. E-mail: alvaro.munoz@uautonoma.cl*

† Electronic supplementary information (ESI) available. See DOI: 10.1039/c8cp04938f

resulting in a Saturn-like molecule. This $C_{50}Cl_{10}$ structure contrasts with the more favorable nearly spherical D_3-C_{50} isomer for the bare C_{50} cage without external groups.[32,33]

The ^{13}C-NMR spectra provide information relevant to the molecular symmetries and chemical environment of each carbon atom in fullerenes.[17,34–37] For C_{60}, owing to its high symmetry, the equivalence of all 60 of its carbon atoms is indicated by the single ^{13}C-NMR resonance at room temperature at 143.15 ppm.[38] At lower temperatures (77 K), the chemical shift anisotropy (CSA) pattern,[36,39] obtained from solid-state NMR experiments, reflects a non-axial symmetry of the chemical environment at the probe nuclei which can be related to the aromatic properties of fullerenes.[40] Thus, the behavior under an external magnetic field provides valuable information about the structure and related properties, which can be generalized over the molecular space by evaluating the induced magnetic field (IMF) from theoretical calculations,[41–43] in addition to the usual probes based on specific NICS calculations at certain sites.[44] Such aromatic properties have been discussed as relevant characteristics in the determination of the structure and reactivity of fullerenes.[45]

Recently, the spherical aromatic character given by the 50π-electron count of the bare C_{50} fullerene in both D_{5h}- and D_3-C_{50} isomers has been revisited,[46,47] in view of the relevant role of the spherical shape in achieving the effective spherical aromatic character expected from the $2(N+1)^2$ Hirsch rule.[48] In this sense, the IMF pattern of D_{5h}-C_{50} exhibits deshielding zones located over the five-membered rings, and shielding zones at the six-membered rings, similar to C_{60},[49] indicating the short-range nature of the response arising from the lack of aromaticity.[47,49] In contrast, D_3-C_{50} exhibits the characteristic shielding cone owing to its spherical aromatic behavior.[47] Herein, we use DFT methods to evaluate further the CSA pattern of the ^{13}C-NMR properties of $C_{50}Cl_{10}$ and the related induced magnetic field. This provides a concise picture of its possible aromatic character in terms of its overall magnetic response, as an extension of the well discussed aromaticity of IPR motifs based on the local response at each ring.[50] In addition, the possibility of fullerenes to undergo bromination[51–54] prompts us to discuss the properties of the related $C_{50}Br_{10}$ counterpart.

Computational details

Geometry optimizations and subsequent calculations were performed at the density functional theory (DFT) level employing the ADF code.[55,56] We used the all-electron triple-ζ Slater basis set augmented with double polarization functions (STO-TZ2P) and the non-local Becke–Perdew (BP86) functional within the generalized gradient approximation (GGA).[57–59] London dispersion corrections to DFT were made using the pairwise method of Grimme (DFT-D3),[60] in addition to the BP86 functional, BP86-D3. The nuclear magnetic shielding tensors were calculated with the NMR module of ADF using gauge-including atomic orbitals (GIAO)[61–64] with the exchange expression proposed by Handy and Cohen,[65] the correlation expression proposed by Perdew, Burke, and Ernzerhof[66] (OPBE), and an all-electron STO-TZ2P basis set. In order to account for the ^{13}C-NMR chemical shift, we used C_{60} as a secondary reference relative to tetramethylsilane (TMS), according to $\delta^{C} = \delta^{C_{60}} + \sigma^{C_{60}} - \sigma^{C}$, where $\delta^{C_{60}} = 143.1$ ppm[36,38] and $\sigma^{C_{60}} = 47.4$ ppm. This approach agrees well with experimental data as observed in previous studies of fused ring systems.[67]

Results and discussion

The $C_{50}Cl_{10}$ structure consists of two facing IPR C_{20} bowls, connected by ten saturated carbon atoms with exohedral –Cl atoms (Fig. 1).[25] The resulting D_{5h} structure shows two corannulene moieties with a bowl depth of 1.500 Å, which is deeper than that of the isolated corannulene molecule ($C_{20}H_{10}$) with a bowl depth of 0.89 Å (exp. 0.87 Å).[68] Four unique carbon atom types are found (Fig. 1), given by C_I, located at the central five-membered ring; C_{II}, as the next type as part of the six-membered rings directly bonded to C_I; C_{III}, as the outer π-carbon atoms; and C_{IV}, as exobonded sp^3-atoms bonded directly to chlorine. The calculated structure for $C_{50}Cl_{10}$ agrees with the X-ray structure reported by Xie and coworkers,[31] showing distances of C_I–C_I = 1.438 Å; C_I–C_{II} = 1.412 Å; C_{II}–C_{III} = 1.433 Å; C_{III}–C_{III} = 1.379 Å; C_{III}–C_{IV} = 1.526 Å; and C_{IV}–C_{IV} = 1.598 Å; with a C_{IV}–Cl distance of 1.814 Å, which are listed in Table 1. The resulting curvature of the IPR motif given by the pyramidalization angles (θ_p) of 12.4°, 10.1° and 9.2° for C_I, C_{II} and C_{III}, respectively, is comparable to that of C_{60} with $\theta_p = 11.6°$. Moreover, the pyramidalization angle of 15.6° for C_{IV} results in an angle of 105.6° between the σ/π orbitals, which is close to the ideal angle of 109.5° for tetrahedral sp^3-carbons. This indicates that such carbon atoms need to be saturated for further kinetic stability. In addition, the $C_{50}Br_{10}$ counterpart exhibits similar carbon–carbon distances, with a very slight shortening of the C_{III}–C_{IV} distances (from 1.525 to 1.517 Å), indicating the rigidity of the IPR dome between chlorinated and brominated species.

The charge distribution along the structure is evaluated by the electrostatic potential (ESP) map, showing that the region at

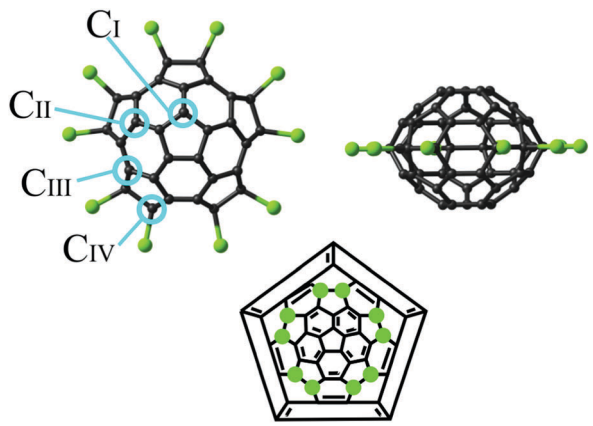

Fig. 1 Two views of $C_{50}Cl_{10}$, along the C_5 and the C_2 axis, and the respective Schlegel diagram with chlorine atoms denoted with lime-green dots. Definition of symmetry equivalent carbon atoms is given for C_I, C_{II}, C_{III} and C_{IV}.

Table 1 Selected distances for studied species. Values in Angstroms (Å)

	$C_{50}Cl_{10}$	$C_{50}Cl_{10}$ (exp.)[a]	$C_{50}Br_{10}$	$C_{30}Cl_{10}H_{10}$
C_I–C_I	1.438	1.435	1.439	1.428
C_I–C_{II}	1.412	1.411	1.411	1.395
C_{II}–C_{III}	1.433	1.415	1.435	1.435
C_{III}–C_{III}	1.383	1.369	1.385	1.392
C_{III}–C_{IV}	1.525	1.543	1.517	1.511
C_{IV}–C_{IV}	1.598	1.589	1.591	1.592
C_{IV}–X	1.814	1.789	2.013	1.816

[a] Data taken from ref. 31.

the molecular equator containing exobonded-carbons exhibits a larger charge, which in turn increases the electron deficiency of the carbons at the IPR dome in comparison to C_{60} (Fig. 2).[69] Such observations suggest enhanced chemistry relative to that of bare fullerenes.[70–73] Interestingly, the equatorial halogen atoms exhibit σ-holes,[74] which can be further used to generate supramolecular structures taking advantage of the two-dimensional five-fold symmetric synthons[75,76] provided by the $C_{50}X_{10}$ species, similarly to that observed for $C_{56}Cl_{10}$.[77]

The ^{13}C-NMR spectra obtained by Xie and coworkers for $C_{50}Cl_{10}$[25] indicate four types of carbon atoms exhibiting resonances at 143.0, 146.6, 161.5 and 88.7 ppm corresponding to the C_I, C_{II}, C_{III} and C_{IV} carbon positions (Fig. 3), respectively. The calculated ^{13}C-NMR chemical shifts at 139.8, 145.5, 166.6 and 88.7 ppm agree well with the reported data (Table 2), where C_I is shielded, and C_{II} and C_{III} are deshielded in comparison to C_{60} (exp. 143.1 ppm).[36,38] The C_{IV} carbon atoms exhibit a chemical shift corresponding to sp^3-carbon atoms. In comparison to the minimal IPR structural motif given by corannulene ($C_{20}H_{10}$), C_I and C_{II} account for the respective hub and rim atoms of corannulene, calculated at 132.7 and 128.2 ppm respectively (exp. 136 and 131 ppm).[39] These are the atoms most sensitive to changes in the IPR curvature, becoming shielded upon planarization (calculated: 132.5 and 126.4 ppm, respectively).[78] In this sense, the values for C_I and C_{II} at 139.8 and 145.5 ppm in $C_{50}Cl_{10}$ are deshielded owing to the increase

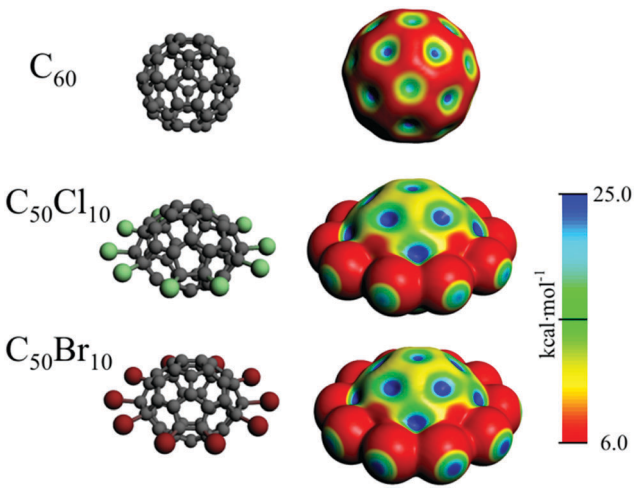

Fig. 2 Electrostatic potential maps of $C_{50}X_{10}$ (X = Cl and Br). The ESP is mapped on isosurfaces of 0.002 a.u. of electron density.

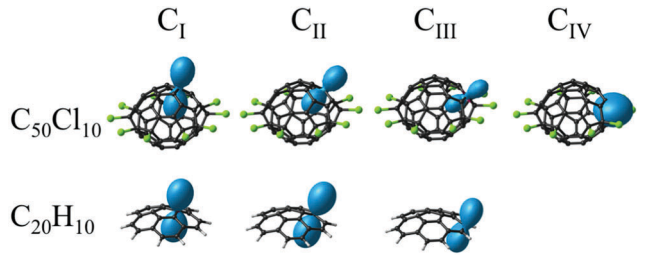

Fig. 3 Orientation and magnitude of the CSA tensor for representative carbon atoms.

Table 2 Calculated CSA parameters obtained at the TZ2P/OPBE level of theory for the studied systems. These involve both anisotropy ($\Delta\sigma$) and asymmetry (η) terms, according to the Haeberlen convention

	σ_{11}	σ_{22}	σ_{33}	σ_{iso}	δ^a	$\delta^{exp.\,b}$	$\Delta\sigma$	η
$C_{50}Cl_{10}$								
C_I	−13.4	−7.9	173.2	50.8	139.8	143.0	181.9	0.05
C_{II}	−18.3	−1.6	155.1	45.1	145.5	146.6	165.0	0.15
C_{III}	−43.2	−18.5	133.5	23.9	166.6	161.5	164.4	0.23
C_{IV}	75.3	106.0	123.5	101.6	89.0	88.7	32.9	1.40
$C_{20}H_{10}$								
C_I	−23.9	18.5	179.0	57.9	132.7	136	181.7	0.35
C_{II}	−8.9	7.2	188.9	62.4	128.2	131	189.8	0.13
C_{III}	−19.8	54.9	162.8	66.0	124.6	126	145.3	0.77
$C_{50}Br_{10}$								
C_I	−12.7	−7.0	172.1	50.8	139.8		181.9	0.05
C_{II}	−18.6	0.5	153.9	45.3	145.3		163.0	0.18
C_{III}	−42.6	−21.1	133.5	23.3	167.3		165.4	0.19
C_{IV}	61.9	110.0	124.4	98.8	91.8		38.5	1.88
$C_{30}Cl_{10}H_{10}$								
C_I	−28.9	−3.8	174.0	47.1	143.5		190.4	0.20
C_{II}	−17.1	−6.7	156.6	44.3	146.3		168.5	0.09
C_{III}	−10.0	28.1	137.6	51.9	138.7		128.5	0.45
C_{IV}	78.5	137.9	143.6	120.0	70.6		35.4	2.52

[a] Chemical shift values relative to fullerene, as a secondary reference according to $\delta^C = \delta^{C_{60}} + \sigma^{C_{60}} - \sigma^C$, where $\delta^{C_{60}}$ = 143.1 ppm and $\sigma^{C_{60}}$ = 47.4 ppm. [b] Experimental chemical shifts from ref. 25 for $C_{50}Cl_{10}$ and from ref. 39 for $C_{20}H_{10}$.

in the IPR curvature (θ_p = 12.4° and 10.1°, respectively) relative to that of $C_{20}H_{10}$ (θ_p = 8.1° and 1.8°, respectively). This observation shows how curvature changes in isolated-pentagon structural motifs in fullerene cages can be evaluated from routine ^{13}C-NMR experiments.

For the hypothetical $C_{50}Br_{10}$ species, the calculated corresponding ^{13}C NMR chemical shifts are 139.8, 145.3, 167.3 and 91.8 ppm, with no change in the C_I chemical shift, small changes less than 1 ppm in the C_{II} and C_{III} chemical shifts, and a change of about 3 ppm in the C_{IV} chemical shift. Such results show that the halogen effect on the ^{13}C-NMR chemical shifts is exhibited mainly in the C_{IV} and C_{III} chemical shifts, leaving almost invariant the IPR dome carbon chemical shifts.

In order to exploit information related to the orientation, magnitude and sign of the nuclear shielding tensor leading to the discussed ^{13}C-NMR values, we provide a graphical representation of the absolute shielding in terms of the chemical shift anisotropy (CSA) in relation to its own principal axis

system (PAS) in Fig. 3.[64,79] This is given by the three principal components (σ_{ij}, i, j = 1, 2, 3) usually discussed in solid-state NMR experiments.[80] Note that such relevant parameters are reduced to a single value (σ_{iso}) when the isotropic representation is employed, accounting for the in-solution molecular tumbling from the ^{13}C-NMR characterization. Here, we follow the Haeberlen convention[81,82] to designate the principal components of the shielding tensor at the nuclei, according to $\sigma_{11} < \sigma_{22} < \sigma_{33}$, with σ_{33} as the more shielded signal, which is useful for our interpretation.

For sp^2-carbon atoms, the main shielded component (σ_{33}) is larger in magnitude and determines the orientation of the shielding tensor, which is oriented perpendicularly to the curved surface (Fig. 3) similar to C_{60} and $C_{20}H_{10}$, among other molecules.[39,40,78,83–85] For $C_{50}Cl_{10}$, the tensor for C_I, C_{II} and C_{III} is more tilted in comparison to the related rim and hub (C_I and C_{II}) carbons of $C_{20}H_{10}$, pointing out that the π-surface curvature is relevant in the resulting orientation of the CSA tensor. The σ_{11} and σ_{22} components appear with lesser magnitude, accounting for the axial-symmetry found in sp^2-carbons ($\sigma_{11} \approx \sigma_{22} \neq \sigma_{33}$). Moreover, for C_{IV}, the principal components tend to more similar values owing to its sp^3 character.

The shape of the CSA tensor can be further analyzed by the anisotropy ($\Delta\sigma$) term within the Haeberlen notation,[81,82] given by $\Delta\sigma = \sigma_{33} - (\sigma_{11} + \sigma_{22})/2$, which exhibits larger values for axially-symmetric tensors (C_I, C_{II} and C_{III}), and lower values for more spherical tensors ($\sigma_{11} \approx \sigma_{22} \approx \sigma_{33}$) as in C_{IV}. Interestingly, comparison of $\Delta\sigma$ for C_{II} between $C_{20}H_{10}$ and $C_{50}Cl_{10}$ suggests that in the more curved π-surface such anisotropy tends to lower values from 189.8 to 165.0 ppm, approaching the C_{60} value of $\Delta\sigma$ = 163.1 ppm (exp.: 163 ppm).[36] Thus, $\Delta\sigma$ provides another indication of the curvature of the π-surface that can be elucidated from solid-state NMR experiments. For $C_{50}Br_{10}$, similar characteristics were obtained from the analysis of the CSA tensors.

Furthermore, the degree of axial-symmetry in sp^2-carbon atoms is provided by the asymmetry (η) term in the Haeberlen notation,[81,82] which accounts for the differences between the σ_{11} and σ_{22} components, as given by $\eta = (\sigma_{22} - \sigma_{11})/(\sigma_{33} - \sigma_{iso})$. The local CSA tensor has been suggested to tend to axial-symmetry in an aromatic structure as shown by the change in η = 0.25 for the non-aromatic C_{60} fullerene, to η = 0.05 for the truly spherical aromatic C_{60}^{10+} counterpart, as evaluated theoretically.[40] For $C_{20}H_{10}$, the η values for C_I and C_{II} are 0.35 and 0.13, respectively, relating to the location of C_I in both antiaromatic five-membered and aromatic six-membered rings in corannulene, but C_{II} only in the aromatic six-membered rings.[78,86] In $C_{50}Cl_{10}$, related C_I and C_{II} values of η are found to be 0.05 and 0.15, respectively, suggesting an aromatic character in the IPR motifs.

In order to provide a concise picture of the possible aromatic character of $C_{50}Cl_{10}$, the induced magnetic field (B^{ind})[41,87] was obtained. This provides regions with shielding and deshielding response close to the molecular space. Under the magnetic criteria of aromaticity,[88] an aromatic system is characterized to exhibit π-electron precession under an external applied magnetic field, which builds up an induced magnetic field opposing or shielding the external field. Moreover, such behaviour is found in different σ-, δ-, electron kernels.[89,90]

For $C_{50}Cl_{10}$ and $C_{50}Br_{10}$, the orientationally averaged magnetic response, $B_{iso}^{ind} = -(1/3)(\sigma_{xx} + \sigma_{yy} + \sigma_{zz})B_j^{ext}$, exhibits a shielding region indicative of an aromatic character as discussed in spherical aromatic fullerenes,[47] and in agreement with the discussion in terms of CSA from the ^{13}C-NMR tensor. Moreover, the representation of B_i^{ind} in terms of specific orientations of the applied field (i = x-, y-, z-axis) provides a detailed picture of the complexity of the induced magnetic response inherent to the studied species. In spherical aromatic fullerenes, the response is similar showing a shielding cone response under any orientation of the applied field. This differs from planar aromatics, in which the shielding cone is obtained under a perpendicularly oriented field.[47,91]

To clarify whether the aromatic behavior has spherical- or planar-aromatic character, a comparison between the response under a perpendicular and parallel field is given. In Fig. 4, the formation of a long-range shielding cone and the respective complementary outer deshielding region under a perpendicularly oriented field (B_z^{ind}) confirms the aromatic character of $C_{50}Cl_{10}$. Such a shielding cone[41,64,92–95] is characteristic of aromatic species, which can be determined from routine NMR experiments.[83,96,97] However, the shielding cone response is not found when the field is oriented parallel (B_x^{ind}; B_y^{ind}), which leads to a short-range shielding response instead, indicative of non-aromatic behavior under such an orientation of the field. This observation interprets $C_{50}Cl_{10}$ and $C_{50}Br_{10}$ as planar-aromatic species rather than spherical-aromatic fullerenes. Moreover, the analysis of one-half of such structures given by $C_{30}Cl_{10}H_{10}$ (ESI,† Tables S1 and S2) reveals similar behavior, exhibiting a long-range shielding cone for B_z^{ind} and a short-range response for B_x^{ind} and B_y^{ind}. At the center of $C_{50}Cl_{10}$ an isotropic shielding value of −17.1 ppm is found, which agrees with the previously reported results by Wang and coworkers (−17.3 ppm).[44] This is larger than that observed for the one-half model (−10.6 ppm), owing to the constructive shielding interaction between IPR structural motifs. This effect is more pronounced when the field is perpendicularly oriented

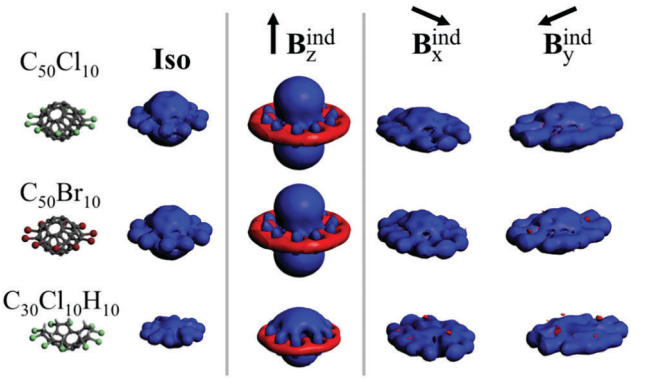

Fig. 4 Three dimensional representation of the magnetic response B^{ind} in relation to the orientational-averaged external field (iso, B_{iso}^{ind}), and specific orientations of the applied field (B_i^{ind}; i = x, y, z). Isosurface values set at 4 ppm relative to the external field.

(B_z^{ind}, related to NICSzz(0)), leading to values of −43.3 and −19.3 ppm, respectively, which are not found for a parallel oriented field (−6.3 and −4.0 ppm, respectively). This indicates that the resulting planar-aromatic behavior of $C_{50}Cl_{10}$ is provided by the sum of the shielding cones of each IPR dome. This is an interesting example of a fullerene in which two approximately hemispherical units are effectively separated by an sp^3-carbon atom "ring", where the resulting aromaticity is an important factor in stabilizing the IPR-violating $C_{50}Cl_{10}$ fullerene.[31] Hence, an expected spherical aromatic fullerene can be converted to a planar-aromatic species by introducing saturation of selected carbon atoms, thereby modifying the induced electron precession along the carbon backbone.

Conclusions

The properties related to the formation of the "saturn-like" $C_{50}Cl_{10}$ fullerene are explored by determining its chemical shift anisotropy patterns related to the previously reported ^{13}C-NMR spectrum. The more curved IPR motif compared with corannulene, resulting in a more curved π-surface, exhibits an interesting variation in the ^{13}C-NMR patterns, where the relation between C_I and C_{II} signals is useful to evaluate the degree of curvature of the π-surface.

The charge distribution of $C_{50}Cl_{10}$ reveals a more electron-deficient IPR dome compared with C_{60}, envisaging an enhanced chemistry relative to bare fullerenes. In addition, the equatorial halogen atoms provide a σ-hole effect, suggesting such oblate fullerenes as interesting two-dimensional five-fold symmetric synthons useful for the formation of supramolecular species. The σ-hole effect is enhanced for the hypothetical $C_{50}Br_{10}$ counterpart as is typical for heavier halogen atoms.

The induced magnetic field suggests that $C_{50}Cl_{10}$ can be considered as an aromatic fullerene, which, despite its closed cage structure, can be better described as a planar-aromatic fullerene. The origin of its aromatic character is given by the face-to-face disposition of two aromatic IPR motifs, separated by a ring of saturated sp^3-carbon atoms. This shows how the functionalization of fullerenes by the introduction of external groups is able to modify the electron delocalization within the fullerene cage.

Conflicts of interest

There are no conflicts to declare.

Acknowledgements

This work was supported by FONDECYT 1180683. We are grateful to Dirección General de Asuntos del Personal Académico (DGAPA) for A. Miralrio postdoctoral fellowship.

References

1 H. W. Kroto, J. R. Heath, S. C. O'Brien, R. F. Curl and R. E. Smalley, C60: Buckminsterfullerene, *Nature*, 1985, **318**, 162–163.
2 R. Taylor, J. P. Hare, A. K. Abdul-Sada and H. W. Kroto, Isolation, separation and characterisation of the fullerenes C60 and C70: the third form of carbon, *J. Chem. Soc., Chem. Commun.*, 1990, 1423.
3 H. W. Kroto, A. W. Allaf and S. P. Balm, C60: Buckminsterfullerene, *Chem. Rev.*, 1991, **91**, 1213–1235.
4 W. Krätschmer, K. Fostiropoulos and D. R. Huffman, The infrared and ultraviolet absorption spectra of laboratory-produced carbon dust: evidence for the presence of the C60 molecule, *Chem. Phys. Lett.*, 1990, **170**, 167–170.
5 H. Kroto, Symmetry, Space, Stars, and C60(Nobel Lecture), *Angew. Chem., Int. Ed. Engl.*, 1997, **36**, 1578–1593.
6 D. H. Parker, P. Wurz, K. Chatterjee, K. R. Lykke, J. E. Hunt, M. J. Pellin, J. C. Hemminger, D. M. Gruen and L. M. Stock, High-yield synthesis, separation, and mass-spectrometric characterization of fullerenes C60 to C266, *J. Am. Chem. Soc.*, 1991, **113**, 7499–7503.
7 W. Wang, J. Dang and X. Zhao, Role of four-membered rings in C32 fullerene stability and mechanisms of generalized Stone-Wales transformation: a density functional theory investigation, *Phys. Chem. Chem. Phys.*, 2011, **13**, 14629.
8 P. W. Fowler and T. Heine, Stabilisation of pentagon adjacencies in the lower fullerenes by functionalisation, *J. Chem. Soc., Perkin Trans. 2*, 2001, 487–490.
9 A. Hirsch, Z. Chen and H. Jiao, Spherical Aromaticity in Ih Symmetrical Fullerenes: The 2(N + 1)2 Rule, *Angew. Chem., Int. Ed.*, 2000, **39**, 3915–3917.
10 K. M. Kadish and R. S. Ruoff, *Fullerenes: Chemistry, Physics, and Technology*, Wiley-Interscience, New York, 2000.
11 M. Bühl and A. Hirsch, Spherical Aromaticity of Fullerenes, *Chem. Rev.*, 2001, **101**, 1153–1184.
12 A. Hirsch and M. Brettreich, *Fullerenes: Chemistry and Reactions*, Wiley-VCH, Weinheim, 2005.
13 P. Schwerdtfeger, L. N. Wirz and J. Avery, The topology of fullerenes, *Wiley Interdiscip. Rev.: Comput. Mol. Sci.*, 2015, **5**, 96–145.
14 R. C. Haddon, L. E. Brus and K. Raghavachari, Electronic structure and bonding in icosahedral C60, *Chem. Phys. Lett.*, 1986, **125**, 459–464.
15 V. Elser and R. C. Haddon, Icosahedral C60: an aromatic molecule with a vanishingly small ring current magnetic susceptibility, *Nature*, 1987, **325**, 792–794.
16 W. Krätschmer, L. D. Lamb, K. Fostiropoulos and D. R. Huffman, Solid C60: a new form of carbon, *Nature*, 1990, **347**, 354–358.
17 C. Piskoti, J. Yarger and A. Zettl, C36, a new carbon solid, *Nature*, 1998, **393**, 771–774.
18 H. Prinzbach, A. Weiler, P. Landenberger, F. Wahl, J. Wörth, L. T. Scott, M. Gelmont, D. Olevano and B. v. Issendorff, Gas-phase production and photoelectron spectroscopy of the smallest fullerene, C20, *Nature*, 2000, **407**, 60–63.
19 Z. Wang, X. Ke, Z. Zhu, F. Zhu, M. Ruan, H. Chen, R. Huang and L. Zheng, A new carbon solid made of the world's smallest caged fullerene C20, *Phys. Lett. A*, 2001, **280**, 351–356.
20 Y. N. Makurin, A. A. Sofronov, A. I. Gusev and A. L. Ivanovsky, Electronic structure and chemical stabilization of C_{28} fullerene, *Chem. Phys.*, 2001, **270**, 293–308.

21 J. M. L. Martin, C28: the smallest stable fullerene?, *Chem. Phys. Lett.*, 1996, **255**, 1–6.
22 H. W. Kroto, The stability of the fullerenes C_n, with n = 24, 28, 32, 36, 50, 60 and 70, *Nature*, 1987, **329**, 529–531.
23 J. Aihara, Y. Nakagami and R. Sekine, Kinetic Stability of Non-IPR Fullerene Molecular Ions, *J. Phys. Chem. A*, 2015, **119**, 6542–6550.
24 J. Aihara, Origin of Kinetic Instability of Fullerenes That Violate the Isolated Pentagon Rule, *J. Phys. Chem. A*, 2015, **119**, 3089–3097.
25 S.-Y. Xie, Capturing the Labile Fullerene[50] as C50Cl10, *Science*, 2004, **304**, 699.
26 L. Xu, X. Shao and W. Cai, Structure, Stability, and Thermochemistry of the Fullerene Derivatives C64X6 (X = H, F, Cl), *J. Phys. Chem. A*, 2009, **113**, 10839–10844.
27 I. S. Neretin, K. A. Lyssenko, M. Y. Antipin, Y. L. Slovokhotov, O. V. Boltalina, P. A. Troshin, A. Y. Lukonin, L. N. Sidorov and R. Taylor, C60F18, a Flattened Fullerene: Alias a Hexa-Substituted Benzene, *Angew. Chem.*, 2000, **39**, 3273–3276.
28 A. G. Avent, O. V. Boltalina, J. M. Street, R. Taylor and X.-W. Wei, The [4+2] cycloaddition of anthracene with C60F18; anthracene goes ring walking, *J. Chem. Soc., Perkin Trans. 2*, 2001, 994–997.
29 S. Jenkins, M. I. Heggie and R. Taylor, Aromaticity of [60]fullerene derivatives (C60Xn, X = H, F; n = 18, 36) constrained to have planar hexagonal rings, *J. Chem. Soc., Perkin Trans. 2*, 2000, 2415–2419.
30 J. Poater, X. Fradera, M. Duran and M. Solà, The Delocalization Index as an Electronic Aromaticity Criterion: Application to a Series of Planar Polycyclic Aromatic Hydrocarbons, *Chem. – Eur. J.*, 2003, **9**, 400–406.
31 X. Han, S. Zhou, Y. Tan, X. Wu, F. Gao, Z. Liao, R. Huang, Y. Feng, X. Lu, S. Xie and L. Zheng, Crystal Structures of Saturn-Like C50Cl10 and Pineapple-Shaped C64Cl4: Geometric Implications of Double- and Triple-Pentagon-Fused Chlorofullerenes, *Angew. Chem., Int. Ed.*, 2008, **47**, 5340–5343.
32 L. Zhechkov, T. Heine and G. Seifert, D 5 h C 50 Fullerene: A Building Block for Oligomers and Solids?, *J. Phys. Chem. A*, 2004, **108**, 11733–11739.
33 X. Lu, Z. Chen, W. Thiel, P. von, R. Schleyer, R. Huang and L. Zheng, Properties of Fullerene[50] and D 5 h Decachlorofullerene[50]: A Computational Study, *J. Am. Chem. Soc.*, 2004, **126**, 14871–14878.
34 J. Kaminský, M. Buděšínský, S. Taubert, P. Bouř and M. Straka, Fullerene C70 characterization by 13C NMR and the importance of the solvent and dynamics in spectral simulations, *Phys. Chem. Chem. Phys.*, 2013, **15**, 9223.
35 T. Heine, M. Bühl, P. W. Fowler and G. Seifert, Modelling the 13C NMR chemical shifts of C84 fullerenes, *Chem. Phys. Lett.*, 2000, **316**, 373–380.
36 C. S. Yannoni, R. D. Johnson, G. Meijer, D. S. Bethune and J. R. Salem, Carbon-13 NMR study of the C60 cluster in the solid state: molecular motion and carbon chemical shift anisotropy, *J. Phys. Chem.*, 1991, **95**, 9–10.
37 R. Tycko, R. C. Haddon, G. Dabbagh, S. H. Glarum, D. C. Douglass and A. M. Mujsce, Solid-state magnetic resonance spectroscopy of fullerenes, *J. Phys. Chem.*, 1991, **95**, 518–520.
38 A. G. Avent, D. Dubois, A. Pénicaud and R. Taylor, The minor isomers and IR spectrum of [84]fullerene, *J. Chem. Soc., Perkin Trans. 2*, 1997, 1907–1910.
39 A. M. Orendt, J. C. Facelli, S. Bai, A. Rai, M. Gossett, L. T. Scott, J. Boerio-Goates, R. J. Pugmire and D. M. Grant, Carbon-13 Shift Tensors in Polycyclic Aromatic Compounds. 8. 1 A Low-Temperature NMR Study of Coronene and Corannulene, *J. Phys. Chem. A*, 2000, **104**, 149–155.
40 A. Muñoz-Castro, Axis-dependent magnetic behavior of C60 and C6010+ consequences of spherical aromatic character, *Chem. Commun.*, 2015, **51**, 10287–10290.
41 R. Islas, T. Heine and G. Merino, The Induced Magnetic Field, *Acc. Chem. Res.*, 2012, **45**, 215–228.
42 E. Kleinpeter, S. Klod and A. Koch, Visualization of through space NMR shieldings of aromatic and anti-aromatic molecules and a simple means to compare and estimate aromaticity, *J. Mol. Struct. THEOCHEM*, 2007, **811**, 45–60.
43 E. Kleinpeter, S. Klod and A. Koch, Endohedral and external through-space shieldings of the fullerenes c50, c60, c60(-6), c70, and c70(-6)-visualization of (anti)aromaticity and their effects on the chemical shifts of encapsulated nuclei, *J. Org. Chem.*, 2008, **73**, 1498–1507.
44 Y. F. Chang, J. P. Zhang, B. Hong, H. Sun, Z. An and R. S. Wang, D5hC50X10: Saturn-like fullerene derivatives (X = F, Cl, Br), *J. Chem. Phys.*, 2005, **123**, 094305.
45 M. Garcia-Borràs, S. Osuna, J. M. Luis, M. Swart and M. Solà, The role of aromaticity in determining the molecular structure and reactivity of (endohedral metallo)fullerenes, *Chem. Soc. Rev.*, 2014, **43**, 5089–5105.
46 A. S. Matías, R. W. A. Havenith, M. Alcamí and A. Ceulemans, Is C 50 a superaromat? Evidence from electronic structure and ring current calculations, *Phys. Chem. Chem. Phys.*, 2016, **18**, 11653–11660.
47 A. Muñoz-Castro, The shielding cone in spherical aromatic structures: insights from models for spherical 2(N + 1)2 aromatic fullerenes, *Phys. Chem. Chem. Phys.*, 2017, **19**, 12633–12636.
48 Z. Chen, H. Jiao, A. Hirsch and W. Thiel, The 2(N + 1)2 rule for spherical aromaticity: further validation, *J. Mol. Model.*, 2001, **7**, 161–163.
49 Z. Chen, J. I. Wu, C. Corminboeuf, J. Bohmann, X. Lu, A. Hirsch and P. von R. Schleyer, Is C60 buckminsterfullerene aromatic?, *Phys. Chem. Chem. Phys.*, 2012, **14**, 14886.
50 E. Steiner, P. W. Fowler and L. W. Jenneskens, Counter-Rotating Ring Currents in Coronene and Corannulene, *Angew. Chem., Int. Ed.*, 2001, **40**, 362–366.
51 P. A. Troshin, D. Kolesnikov, A. V. Burtsev, R. N. Lubovskaya, N. I. Denisenko, A. A. Popov, S. I. Troyanov and O. V. Boltalina, Bromination of [60]Fullerene. I. High-Yield Synthesis of $C_{60}Br_x$ (x = 6, 8, 24), *Fullerenes, Nanotubes, Carbon Nanostruct.*, 2003, **11**, 47–60.
52 F. Cataldo, O. Ursini and P. Ragni, Ultrasound-assisted Bromination. Part 1: Bromination of C 60 and C 70, *Fullerenes, Nanotubes, Carbon Nanostruct.*, 2013, **21**, 346–356.

53 A. A. Popov, V. M. Senyavin and A. A. Granovsky, Vibrational Spectra of Chloro- and Bromofullerenes, *Fullerenes, Nanotubes, Carbon Nanostruct.*, 2005, **12**, 305–310.
54 T. S. Papina, V. A. Luk'yanova, S. I. Troyanov, A. V. Burtsev, M. G. Serov, V. A. Ioutsi, A. G. Buyanovskaya and O. A. Levinskaya, Standard enthalpy of formation of fullerene bromide C60Br24, *Moscow Univ. Chem. Bull.*, 2013, **68**, 12–16.
55 Amsterdam Density Functional (ADF 2016) Code, Vrije Universiteit, Amsterdam, The Netherlands, available at: http://www.scm.com.
56 G. te Velde, F. M. Bickelhaupt, E. J. Baerends, C. Fonseca Guerra, S. J. A. van Gisbergen, J. G. Snijders, T. Ziegler, G. T. E. Velde, C. F. Guerra and S. J. A. Gisbergen, Chemistry with ADF, *J. Comput. Chem.*, 2001, **22**, 931–967.
57 A. D. Becke, Density-functional exchange-energy approximation with correct asymptotic behavior, *Phys. Rev. A: At., Mol., Opt. Phys.*, 1988, **38**, 3098–3100.
58 J. P. Perdew, Density-functional approximation for the correlation energy of the inhomogeneous electron gas, *Phys. Rev. B: Condens. Matter Mater. Phys.*, 1986, **33**, 8822–8824.
59 S. H. Vosko, L. Wilk and M. Nusair, Accurate spin-dependent electron liquid correlation energies for local spin density calculations: a critical analysis, *Can. J. Phys.*, 1980, **58**, 1200–1211.
60 S. Grimme, Density functional theory with London dispersion corrections, *Wiley Interdiscip. Rev.: Comput. Mol. Sci.*, 2011, **1**, 211–228.
61 K. Wolinski, J. F. Hinton and P. Pulay, Efficient implementation of the gauge-independent atomic orbital method for NMR chemical shift calculations, *J. Am. Chem. Soc.*, 1990, **112**, 8251–8260.
62 G. Schreckenbach and T. Ziegler, Calculation of NMR Shielding Tensors Using Gauge-Including Atomic Orbitals and Modern Density Functional Theory, *J. Phys. Chem.*, 1995, **99**, 606–611.
63 S. K. Wolff, T. Ziegler, E. van Lenthe and E. J. Baerends, Density functional calculations of nuclear magnetic shieldings using the zeroth-order regular approximation (ZORA) for relativistic effects: ZORA nuclear magnetic resonance, *J. Chem. Phys.*, 1999, **110**, 7689.
64 M. Kaupp, M. Bühl and V. G. Malkin, *Calculation of NMR and EPR parameters: theory and applications*, John Wiley & Sons, Inc., 2006.
65 N. C. Handy and A. J. Cohen, Left-right correlation energy, *Mol. Phys.*, 2001, **99**, 403–412.
66 J. P. Perdew, K. Burke and M. Ernzerhof, Generalized gradient approximation made simple, *Phys. Rev. Lett.*, 1996, **77**, 3865–3868.
67 J. Camacho Gonzalez and A. Muñoz-Castro, Alternation of aromatic–nonaromatic rings in belt-like structures. The behavior of [6.8] 3 cyclacene in magnetic fields, *Phys. Chem. Chem. Phys.*, 2015, **17**, 17023–17026.
68 J. C. Hanson and C. E. Nordman, The crystal and molecular structure of corannulene, C20H10, *Acta Crystallogr., Sect. B: Struct. Crystallogr. Cryst. Chem.*, 1976, **32**, 1147–1153.
69 P. W. Fowler and A. Ceulemans, Electron Deficiency of the Fullerenes, *J. Phys. Chem.*, 1995, **99**, 508–510.
70 A. L. Balch and M. M. Olmstead, Reactions of Transition Metal Complexes with Fullerenes (C60, C70, *etc.*) and Related Materials, *Chem. Rev.*, 1998, **98**, 2123–2166.
71 D. V. Konarev and R. N. Lyubovskaya, New approaches to the synthesis of transition-metal complexes of fullerenes C60 and C70, *Russ. Chem. Rev.*, 2016, **85**, 1215–1228.
72 Y. Rubin, in *Fullerenes and Related Structures*, ed. A. Hirsch, Springer, Berlin, Heidelberg, 1999, pp. 67–91.
73 A. Hirsch and M. Brettreich, *Fullerenes*, Wiley-VCH Verlag GmbH & Co. KGaA, Weinheim, FRG, 2004.
74 X. Yang, C.-X. Yan, F. Yang, D.-G. Zhou, P.-P. Zhou and S. Liu, Linear σ-Hole Bonding Dimers and Trimers Between Dihalogen Molecules XY (X, Y = Cl, Br) and Carbon Monoxide, *ChemistrySelect*, 2017, **2**, 2687–2699.
75 D. S. Reddy, D. C. Craig and G. R. Desiraju, Supramolecular Synthons in Crystal Engineering. 4. Structure Simplification and Synthon Interchangeability in Some Organic Diamondoid Solids, *J. Am. Chem. Soc.*, 1996, **118**, 4090–4093.
76 G. R. Desiraju, Supramolecular Synthons in Crystal Engineering—A New Organic Synthesis, *Angew. Chem., Int. Ed. Engl.*, 1995, **34**, 2311–2327.
77 Y.-Z. Tan, X. Han, X. Wu, Y.-Y. Meng, F. Zhu, Z.-Z. Qian, Z.-J. Liao, M.-H. Chen, X. Lu, S.-Y. Xie, R.-B. Huang and L.-S. Zheng, An Entrant of Smaller Fullerene: C 56 Captured by Chlorines and Aligned in Linear Chains, *J. Am. Chem. Soc.*, 2008, **130**, 15240–15241.
78 A. Muñoz-Castro, W. Caimanque-Aguilar and C. Morales-Verdejo, Computational Study of 13C NMR Chemical Shift Anisotropy Patterns in C20H10 and [C20H10]4-. Insights into Their Variation upon Planarization and Formation of Concentric Aromatic Species in the Smaller Isolated-Pentagon Structural Motif, *J. Phys. Chem. A*, 2017, **121**, 2698–2703.
79 M. Kaupp, *Calculation of NMR and EPR Parameters*, Wiley-VCH Verlag GmbH & Co. KGaA, Weinheim, FRG, 2004, pp. 293–306.
80 F. Ziarelli and S. Caldarelli, Solid-state NMR as an analytical tool: quantitative aspects, *Solid State Nucl. Magn. Reson.*, 2006, **29**, 214–218.
81 R. K. Harris, E. D. Becker, S. M. Cabral de Menezes, P. Granger, R. E. Hoffman and K. W. Zilm, Further conventions for NMR shielding and chemical shifts (IUPAC Recommendations 2008), *Pure Appl. Chem.*, 2008, **80**, 59–84.
82 U. Haeberlen, High Resolution NMR in Solids: Selective Averaging, *Advances in Magnetic Resonance*, Academic Press, New York, 1976.
83 T. Heine, C. Corminboeuf, G. Grossmann and U. Haeberlen, Proton Magnetic Shielding Tensors in Benzene—From the Individual Molecule to the Crystal, *Angew. Chem., Int. Ed.*, 2006, **45**, 7292–7295.
84 E. Zurek and J. Autschbach, Density Functional Calculations of the ^{13}C NMR Chemical Shifts in (9,0) Single-Walled Carbon Nanotubes, *J. Am. Chem. Soc.*, 2004, **126**, 13079–13088.
85 E. Zurek, C. J. Pickard and J. Autschbach, Density Functional Study of the ^{13}C NMR Chemical Shifts in

Single-Walled Carbon Nanotubes with Stone–Wales Defects, *J. Phys. Chem. C*, 2008, **112**, 11744–11750.
86 A. Ayalon, M. Rabinovitz, P.-C. Cheng and L. T. Scott, Corannulene Tetraanion: A Novel Species with Concentric Anionic Rings, *Angew. Chem., Int. Ed. Engl.*, 1992, **31**, 1636–1637.
87 G. Merino, T. Heine and G. Seifert, The Induced Magnetic Field in Cyclic Molecules, *Chem. – Eur. J.*, 2004, **10**, 4367–4371.
88 R. Gershoni-Poranne and A. Stanger, Magnetic criteria of aromaticity, *Chem. Soc. Rev.*, 2015, **44**, 6597–6615.
89 D. Y. Zubarev, B. B. Averkiev, H.-J. Zhai, L.-S. Wang and A. I. Boldyrev, Aromaticity and antiaromaticity in transition-metal systems, *Phys. Chem. Chem. Phys.*, 2008, **10**, 257–267.
90 W. Yamaguchi, δ and σ *vs.* π conflicting aromatic pentagonal ring of tungsten with a planar pentacoordinate carbon at the ring center, *Int. J. Quantum Chem.*, 2009, 1086–1091.
91 P. R. von Schleyer and H. Jiao, What is aromaticity?, *Pure Appl. Chem.*, 1996, **68**, 209–218.
92 J. A. N. F. Gomes and R. B. Mallion, Aromaticity and Ring Currents, *Chem. Rev.*, 2001, **101**, 1349–1384.
93 D. Sitkoff and D. A. Case, Theories of chemical shift anisotropies in proteins and nucleic acids, *Prog. Nucl. Magn. Reson. Spectrosc.*, 1998, **32**, 165–190.
94 D. A. Case, The use of chemical shifts and their anisotropies in biomolecular structure determination, *Curr. Opin. Struct. Biol.*, 1998, **8**, 624–630.
95 T. Heine, C. Corminboeuf and G. Seifert, The Magnetic Shielding Function of Molecules and Pi-Electron Delocalization, *Chem. Rev.*, 2005, **105**, 3889–3910.
96 A. B. Sahakyan and M. Vendruscolo, Analysis of the Contributions of Ring Current and Electric Field Effects to the Chemical Shifts of RNA Bases, *J. Phys. Chem. B*, 2013, **117**, 1989–1998.
97 J. A. Platts and K. Gkionis, NMR shielding as a probe of intermolecular interactions: ab initio and density functional theory studies, *Phys. Chem. Chem. Phys.*, 2009, **11**, 10331.

